Supplementary Information

Structuring lipid nanoparticles, DNA, and protein corona into stealth bionanoarchitectures for in vivo gene delivery

Serena Renzi,[1#] Luca Digiacomo,[1#] Daniela Pozzi,[1#] Erica Quagliarini,[1] Elisabetta Vulpis,[1] Maria Valeria Giuli,[2] Angelica Mancusi,[1] Bianca Natiello,[1] Maria Gemma Pignataro,[3] Gianluca Canettieri,[1] Laura Di Magno,[1] Luca Pesce,[4] Valentina De Lorenzi,[4] Samuele Ghignoli,[4] Luisa Loconte,[1] Carmela Maria Montone[5], Anna Laura Capriotti,[5] Aldo Laganà,[5] Carmine Nicoletti,[6] Heinz Amenitsch,[7] Marco Rossi,[8] Francesco Mura,[8] Giacomo Parisi,[8] Francesco Cardarelli,[4] Alessandra Zingoni,[1]* Saula Checquolo,[2]* Giulio Caracciolo[1]*

[1]*Department of Molecular Medicine, Sapienza University of Rome, 00161 Rome, Italy*
[2]*Department of Medico-Surgical Sciences and Biotechnology, Sapienza University of Rome, Laboratory affiliated to Istituto Pasteur Italia-Fondazione Cenci Bolognetti, 04100 Latina, Italy*
[3]*Department of Radiological, Oncological and Pathological Sciences, Sapienza University of Rome, 00161, Rome, Italy*
[4]*NEST, Scuola Normale Superiore, 56127 Pisa, Italy*
[5]*Department of Chemistry, Sapienza University of Rome, 00185 Rome, Italy*
[6]*Unit of Histology and Medical Embryology, Department of Anatomy, Histology, Forensic Medicine and Orthopedics, Sapienza University of Rome, 00161 Rome, Italy*
[7]*Institute of Inorganic Chemistry, Graz University of Technology, 8010 Graz, Austria*
[8] *Department of Basic and Applied Sciences for Engineering and Center for Nanotechnology Applied to Engineering (CNIS), Sapienza University of Rome, Via Antonio Scarpa 16, 00161 Rome, Italy*

#equal contributions

Corresponding Authors*****
Alessandra Zingoni (AZ): alessandra.zingoni@uniroma1.it
Saula Checquolo (SC): saula.checquolo@uniroma1.it
Giulio Caracciolo (GC): giulio.caracciolo@uniroma1.it

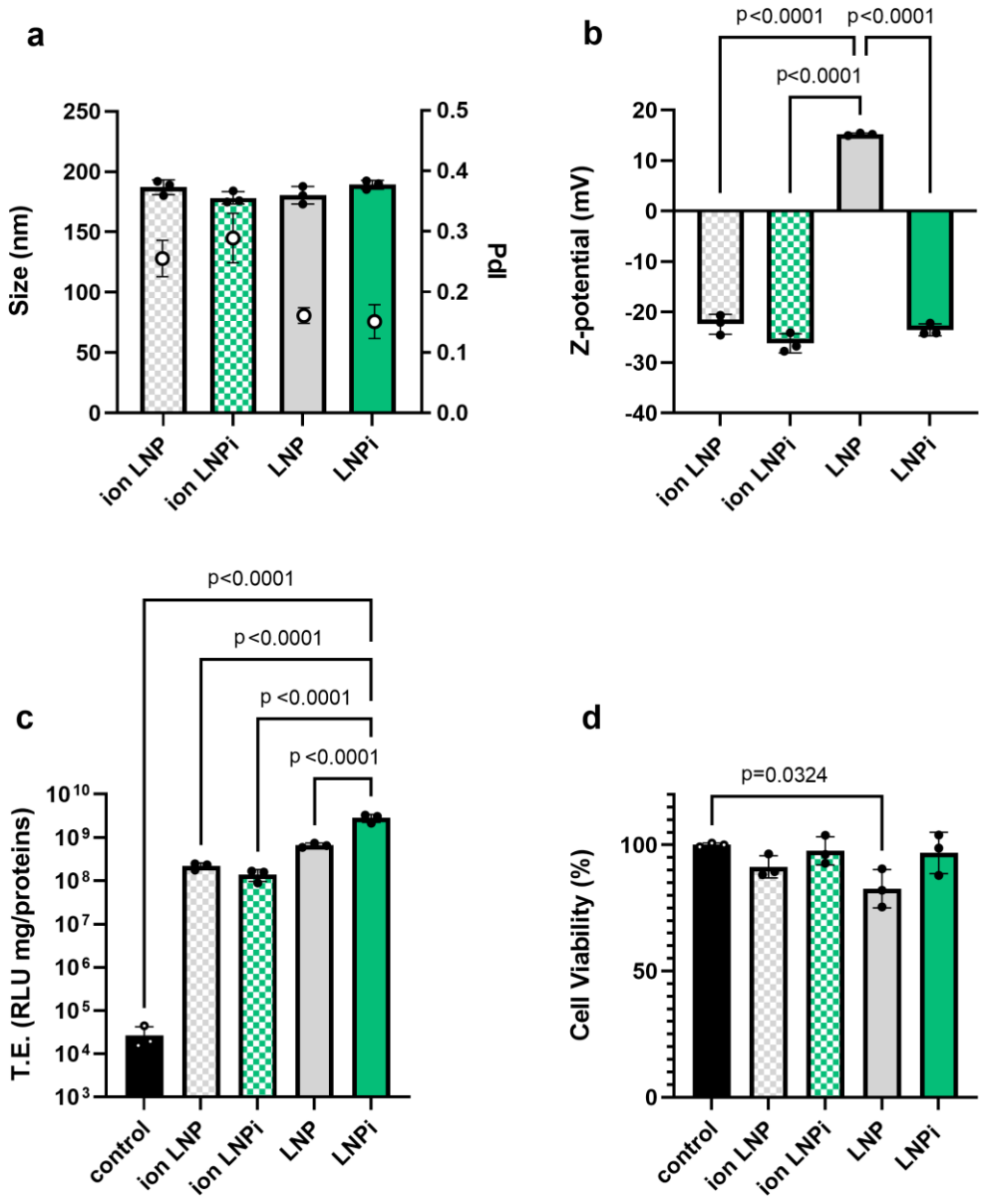

Supplementary Figure 1. (a) Physical-chemical characterization in terms of size, PdI and (b) Z-potential of plain ionizable LNP (ion LNP) (patterned grey) and ion LNPi coated with an intermediate amount of pDNA (patterned green). Results are reported as mean ± standard deviation of three repeated measurements. Statistical analysis was performed by one-way ANOVA test followed by Tukey's multiple-comparison test. P-values < 0.05 are reported. (c) Transfection efficiency of ion LNP and ion LNPi and (d) cell viability measured after 48h from treatment. Results are reported as mean ± standard deviation of three independent measurements. Statistical analysis was performed by one-way ANOVA test followed by Tukey's multiple-comparison test. P-values < 0.05 are reported. LNP and LNPi containing permanently cationic lipids were used as comparison. Source data are provided as a Source Data file.

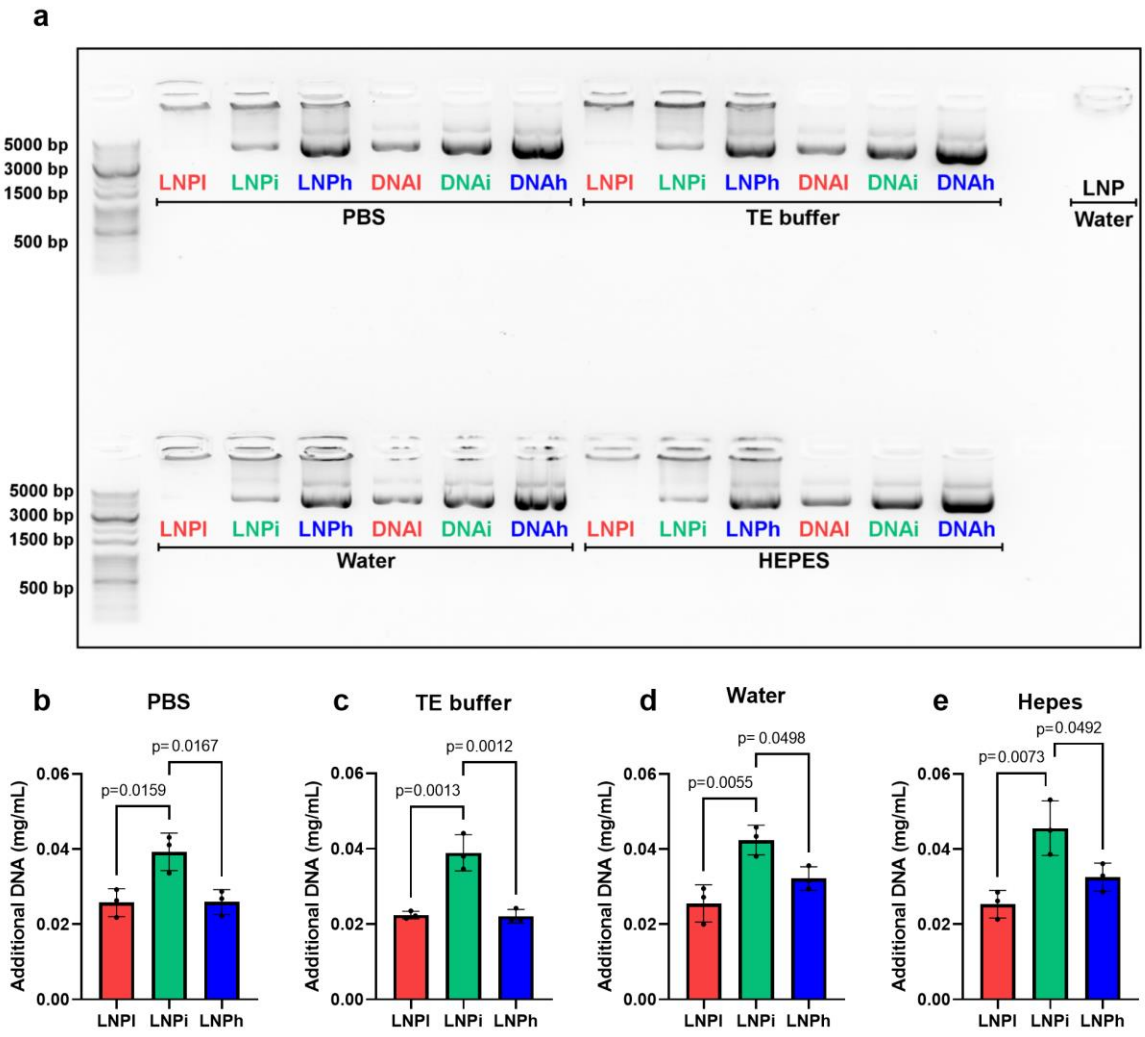

Supplementary Figure 2. (a) Image of agarose gel loaded with LNPs prepared in different buffers, namely PBS, TE buffer, water, and HEPES, with distinct DNA coating levels categorized as low (l), intermediate (i), and high (h), referred to as LNPl, LNPi, and LNPh, respectively. DNAl, DNAi, and DNAh represent the corresponding amounts of free DNA equivalent to those coated on LNPl, LNPi, and LNPh. Additionally, DNA ladder and LNPs without DNA coating were included as references. Band intensity analysis was conducted to evaluate additional DNA binding to LNPs across samples in (b) PBS, (c) TE buffer, (d) water, and (e) HEPES. Statistical analysis was performed by one-way ANOVA test followed by Tukey's multiple-comparison test (n=3 repeated measurements). P-values < 0.05 are reported. The reduction in band intensities observed in each of LNPl, LNPi, and LNPh compared to DNA references confirms the binding of DNA to the LNP surface, resulting in limited electrophoretic mobility. This observation underscores the stability of the LNP platform, which is maintained irrespective of the dilution solvent, and is indicative of the strong electrostatic interaction between the negative charge of DNA and the cationic lipid shell. Source data are provided as a Source Data file.

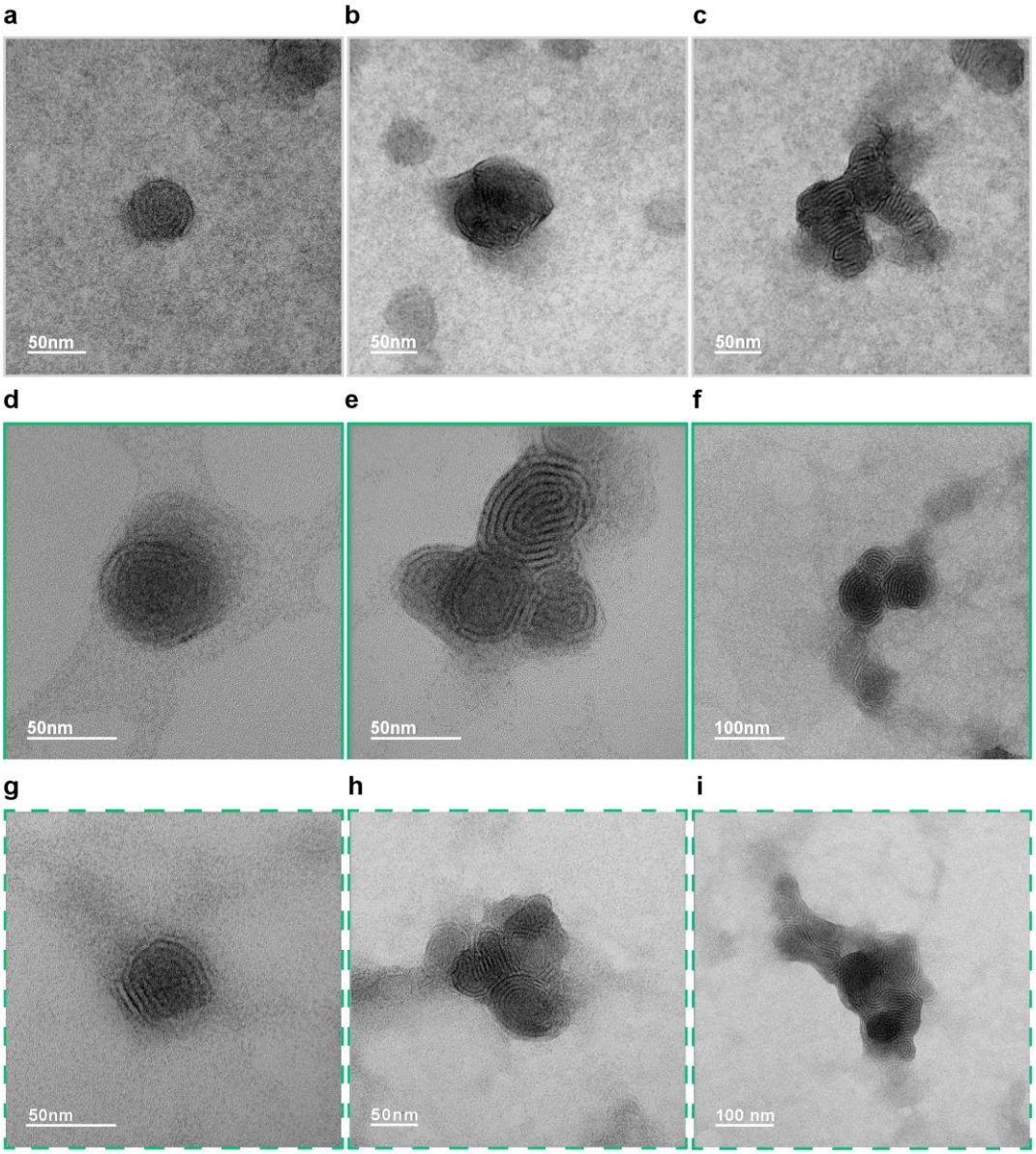

Supplementary Figure 3. Representative TEM images of LNP (panels a-c), LNPi (panels d-f), and coronated LNPi (panels g-i). The borders of the TEM images align with the color scheme employed consistently in the manuscript, where LNP is represented in gray, LNPi is depicted in light green, and coronated LNPi is indicated in patterned green. Source data are provided as a Source Data file.

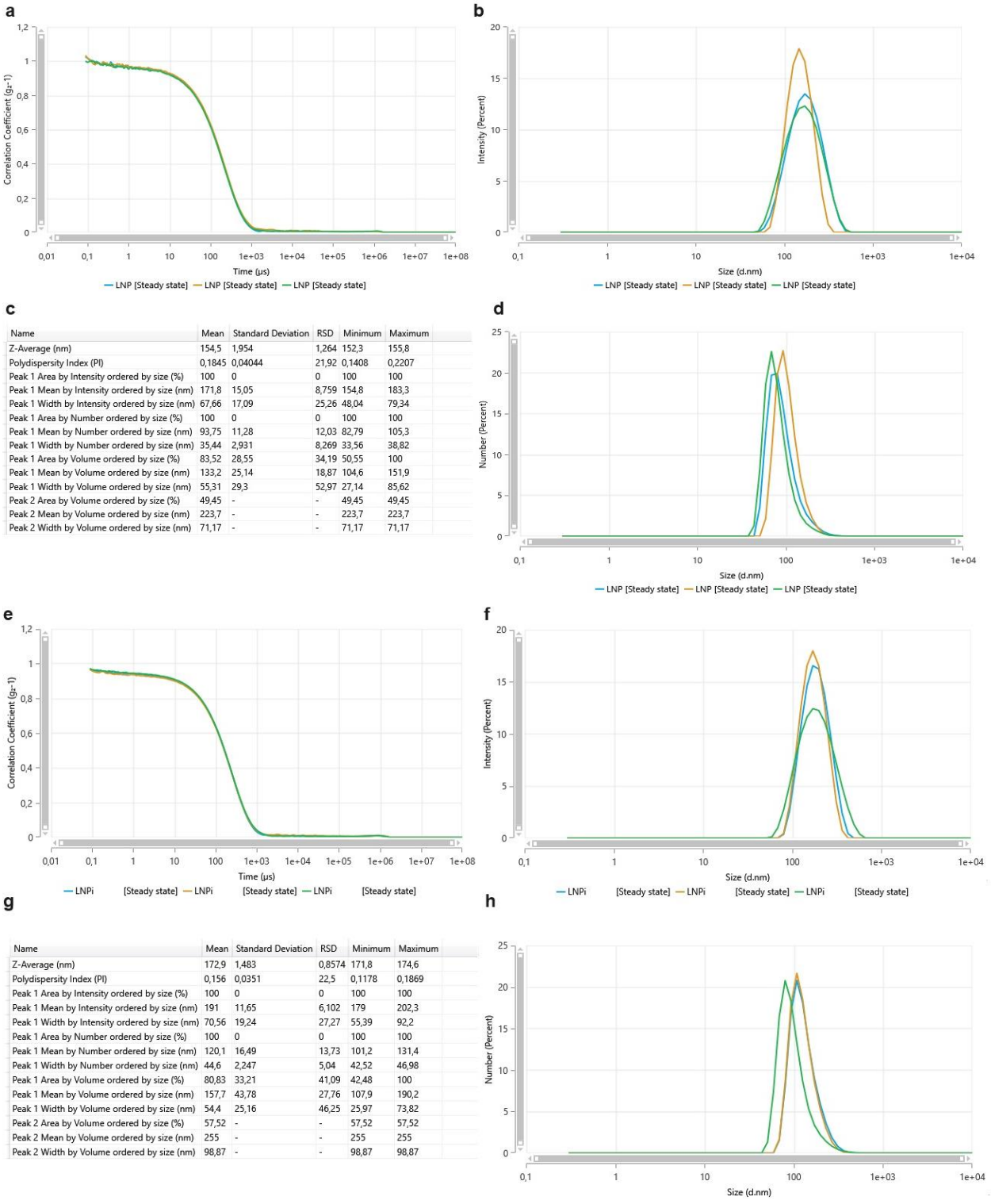

Name	Mean	Standard Deviation	RSD	Minimum	Maximum
Z-Average (nm)	154,5	1,954	1,264	152,3	155,8
Polydispersity Index (PI)	0,1845	0,04044	21,92	0,1408	0,2207
Peak 1 Area by Intensity ordered by size (%)	100	0	0	100	100
Peak 1 Mean by Intensity ordered by size (nm)	171,8	15,05	8,759	154,8	183,3
Peak 1 Width by Intensity ordered by size (nm)	67,66	17,09	25,26	48,04	79,34
Peak 1 Area by Number ordered by size (%)	100	0	0	100	100
Peak 1 Mean by Number ordered by size (nm)	93,75	11,28	12,03	82,79	105,3
Peak 1 Width by Number ordered by size (nm)	35,44	2,931	8,269	33,56	38,82
Peak 1 Area by Volume ordered by size (%)	83,52	28,55	34,19	50,55	100
Peak 1 Mean by Volume ordered by size (nm)	133,2	25,14	18,87	104,6	151,9
Peak 1 Width by Volume ordered by size (nm)	55,31	29,3	52,97	27,14	85,62
Peak 2 Area by Volume ordered by size (%)	49,45	-	-	49,45	49,45
Peak 2 Mean by Volume ordered by size (nm)	223,7	-	-	223,7	223,7
Peak 2 Width by Volume ordered by size (nm)	71,17	-	-	71,17	71,17

Name	Mean	Standard Deviation	RSD	Minimum	Maximum
Z-Average (nm)	172,9	1,483	0,8574	171,8	174,6
Polydispersity Index (PI)	0,156	0,0351	22,5	0,1178	0,1869
Peak 1 Area by Intensity ordered by size (%)	100	0	0	100	100
Peak 1 Mean by Intensity ordered by size (nm)	191	11,65	6,102	179	202,3
Peak 1 Width by Intensity ordered by size (nm)	70,56	19,24	27,27	55,39	92,2
Peak 1 Area by Number ordered by size (%)	100	0	0	100	100
Peak 1 Mean by Number ordered by size (nm)	120,1	16,49	13,73	101,2	131,4
Peak 1 Width by Number ordered by size (nm)	44,6	2,247	5,04	42,52	46,98
Peak 1 Area by Volume ordered by size (%)	80,83	33,21	41,09	42,48	100
Peak 1 Mean by Volume ordered by size (nm)	157,7	43,78	27,76	107,9	190,2
Peak 1 Width by Volume ordered by size (nm)	54,4	25,16	46,25	25,97	73,82
Peak 2 Area by Volume ordered by size (%)	57,52	-	-	57,52	57,52
Peak 2 Mean by Volume ordered by size (nm)	255	-	-	255	255
Peak 2 Width by Volume ordered by size (nm)	98,87	-	-	98,87	98,87

Supplementary Figure 4. Correlation functions of LNP (a) and LNPi (e) measurements. Intensity size distribution of LNP (b) and LNPi (f) along with the number distribution (d and h for LNP and LNPi respectively). Statistical table of size measurement for plain LNP (c) and DNA coated LNP (g).

Supplementary Table 1. NTA analysis of LNP and LNPi. D10, D50, and D90 are parameters that describe the size distribution of particles in a sample. D10 (nm): Indicates the diameter below which 10% of the total volume of particles is found; D50 (nm): Also known as the median diameter, represents the diameter below which 50% of the total volume of particles is found. It is the median value of the particle size distribution. 50% of the particles have a diameter smaller than this value, and the remaining 50% have a diameter larger; D90 (nm): Indicates the diameter below which 90% of the total volume of particles is found.

	Mode (nm)	**Mean (nm)**	**Standard dev. (nm)**	**D10 (nm)**	**D50 (nm)**	**D90 (nm)**	**Concentration (particles/mL)**	**Span**
LNP	72.5	107	97	50	83	179	3.23E+12	1.55
LNPi	72.5	133	99	57	107	231	3.34E+12	1.62

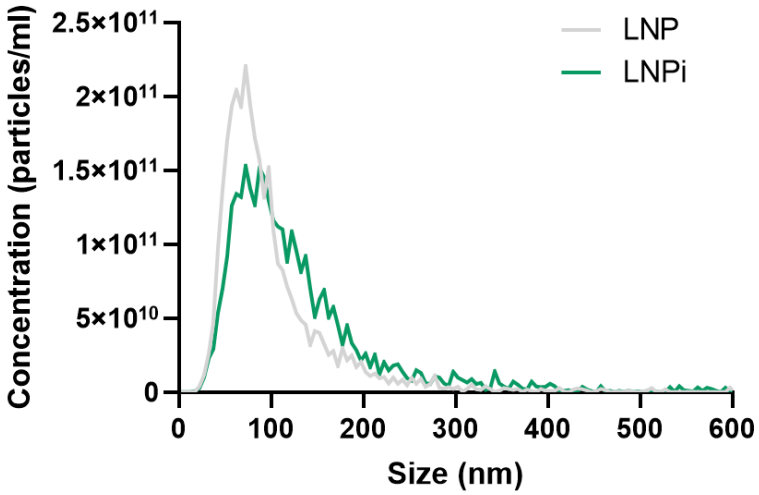

Supplementary Figure 5: Size and particle concentration of LNP, LNPi and coronated LNPi. Equal concentration of starting LNP was incubated with PBS1x or DNA. The size (nm) distribution and the resulted particle concentration evaluated using Nanosight Pro (Malvern, UK) have been reported for both samples. Source data are provided as a Source Data file.

Supplementary Table 2. **Size, polysdispersity (PdI) index and zeta potential of DNA-coated LNP**s. DNA-coated LNPs were generated using functional DNA (i.e. coding for firefly luciferase) and subsequently were incubated with varying concentrations of DNA (0.1 mg/ml, 0.2 mg/ml, and 0.3 mg/ml. This procedure resulted in three distinct categories of LNPs characterized by low (LNPl), intermediate (LNPi), and high (LNPh) DNA coating. To elucidate the impact of surface-bound DNA on the structure and function of DNA-coated LNPs, a series of variants was prepared using non-functional DNA (yellow in the sketch below). These particles were subsequently coated with functional DNA, denoted as LNPl nf-DNA, LNPi, and LNPh, to explore the intricate relationship between surface-bound DNA and the structural-functional attributes of LNPs. The schematic reported in Figure 3a in the main text illustrates the distinct composition of LNPs encapsulating functional DNA as opposed to nonfunctional DNA, focusing on LNPs with an intermediate DNA coating (LNPi).

	Size (nm)	PdI	Z potential (mV)	Z deviation (mV)
LNP	178 ± 5	0.161 ± 0.013	15.4 ± 0.2	5.2 ± 0.4
LNPl	192 ± 5	0.147 ± 0.014	-7.4 ± 3.8	8.7 ± 2.3
LNPi	189 ± 5	0.151 ± 0.028	-23.4 ± 1.1	6.1 ± 0.3
LNPh	178 ± 6	0.257 ± 0.010	-30.5 ± 0.9	7.8 ± 0.2
LNP nf-DNA	154 ± 1	0.240 ± 0.008	18.9 ± 0.4	5.1 ± 0.4
LNPl nf-DNA	216 ± 4	0.289 ± 0.031	-7.9 ± 1.4	5.9 ± 0.8
LNP nf-DNA	209 ± 7	0.226 ± 0.022	-23.5 ± 1.4	4.5 ± 0.2
LNPh nf-DNA	228 ± 10	0.273 ± 0.039	-37.0 ± 17.8	7.6 ± 0.7

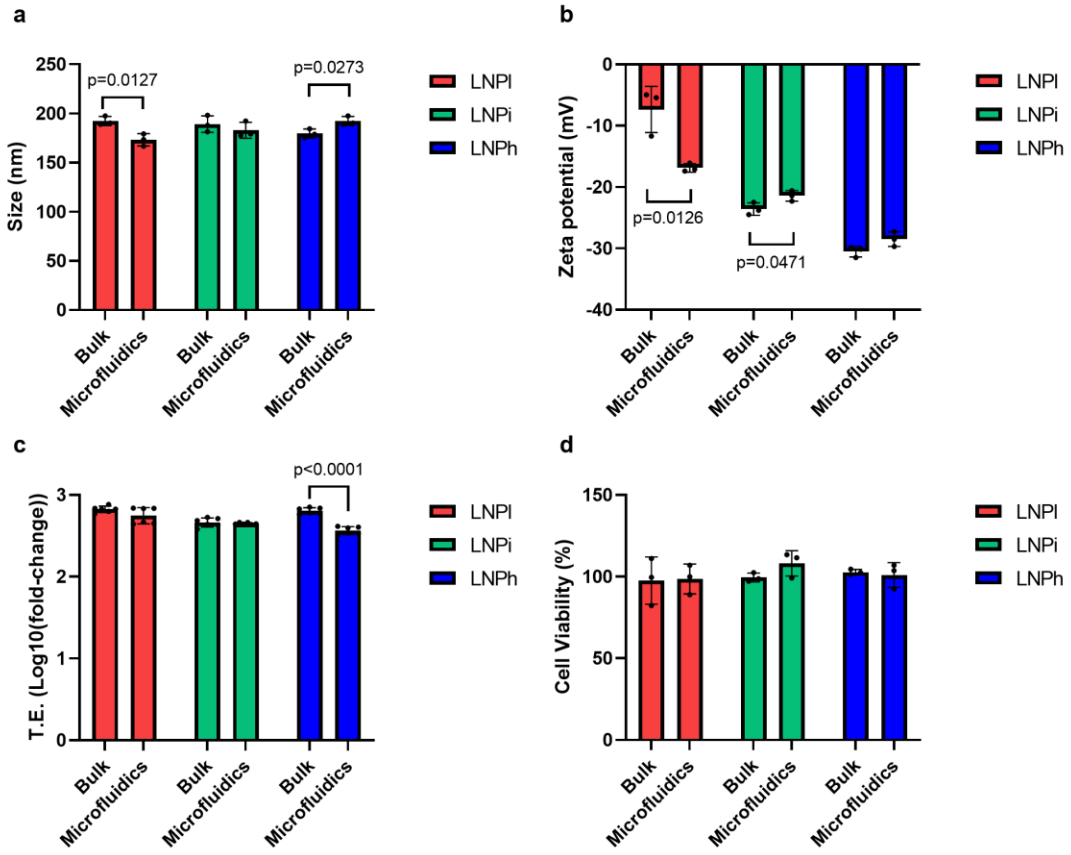

Supplementary Figure 6. Comparison between microfluidic-generated LNPs decorated with DNA using either bulk mixing or an additional microfluidic mixing step, focusing on (a) size (n=3 repeated measurements), (b) Z-potential (n=3 repeated measurements), (c) Transfection Efficiency (TE) (n=6 independent measurements), and (d) Cell Viability (n=3 independent measurements). TE and cell viability were measured 48 hours after treatment of HEK-293 cells. Statistical significance between bulk and microfluidics groups has been evaluated by two-tailed unpaired Student's t-test. P-values <0.05 are reported. As the additional microfluidic mixing step did not improve the physicochemical features or the efficiency of DNA-coated LNPs, bulk mixing was further employed for the development of the DNA-coated systems. Source data are provided as a Source Data file.

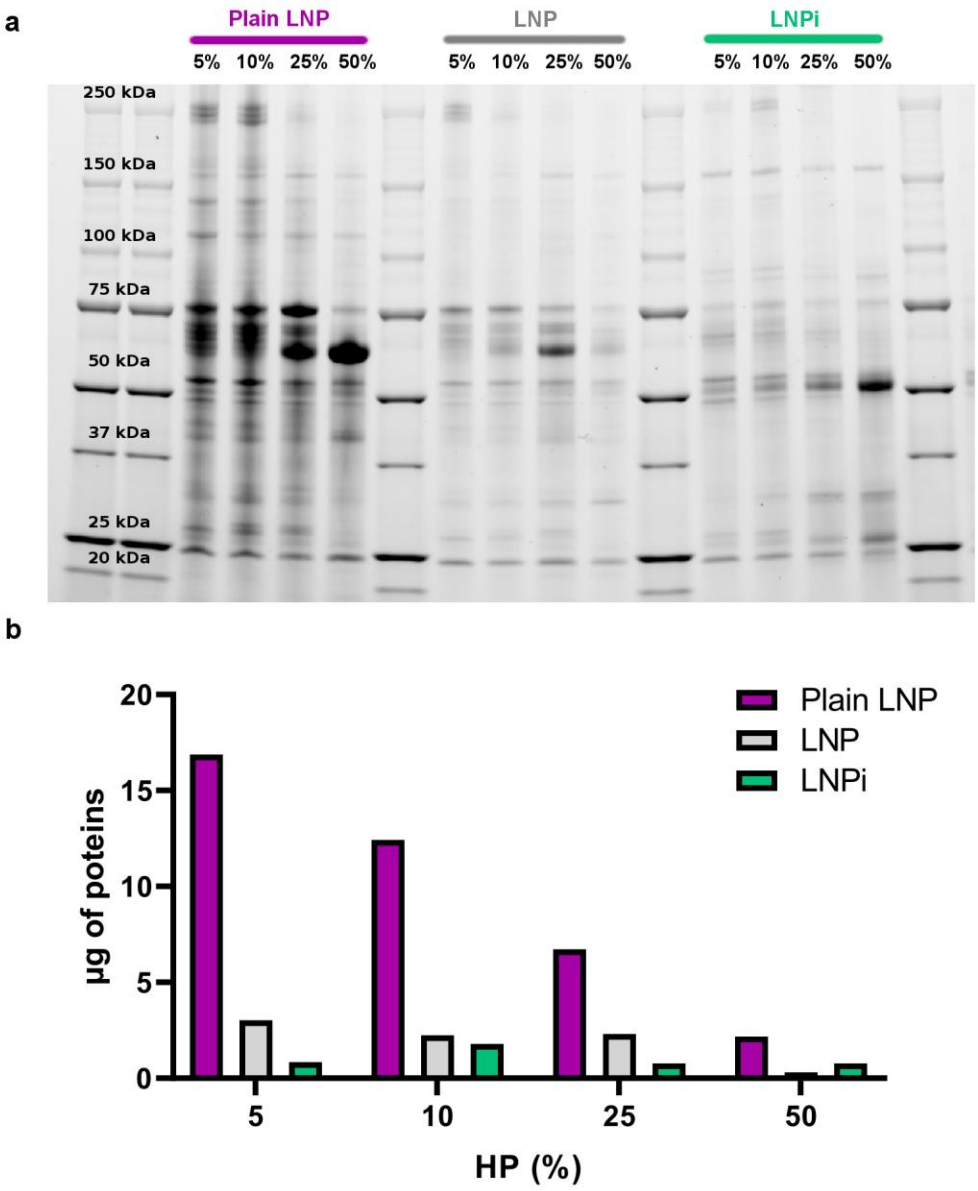

Supplementary Figure 7. (a) One-dimensional SDS-PAGE gel of human plasma (HP) proteins obtained from plain LNP, LNP and LNPi. following incubation at different plasma concentrations. The molecular weights of the proteins in the standard ladder are provided as reference points on the initial two lanes to the left and the last lane on the right. Increasing the number of standard ladders enhances the precision of data and strengthens the reliability of conclusions drawn from the 1D protein profiles obtained from the gel lanes. (b) Micrograms of proteins bound to LNPs after 1 h incubation with HP as determined by Bicinchoninic acid (BCA) assay: plain LNP (purple bars), LNP (gray bars), LNPi (green bars). Source data are provided as a Source Data file.

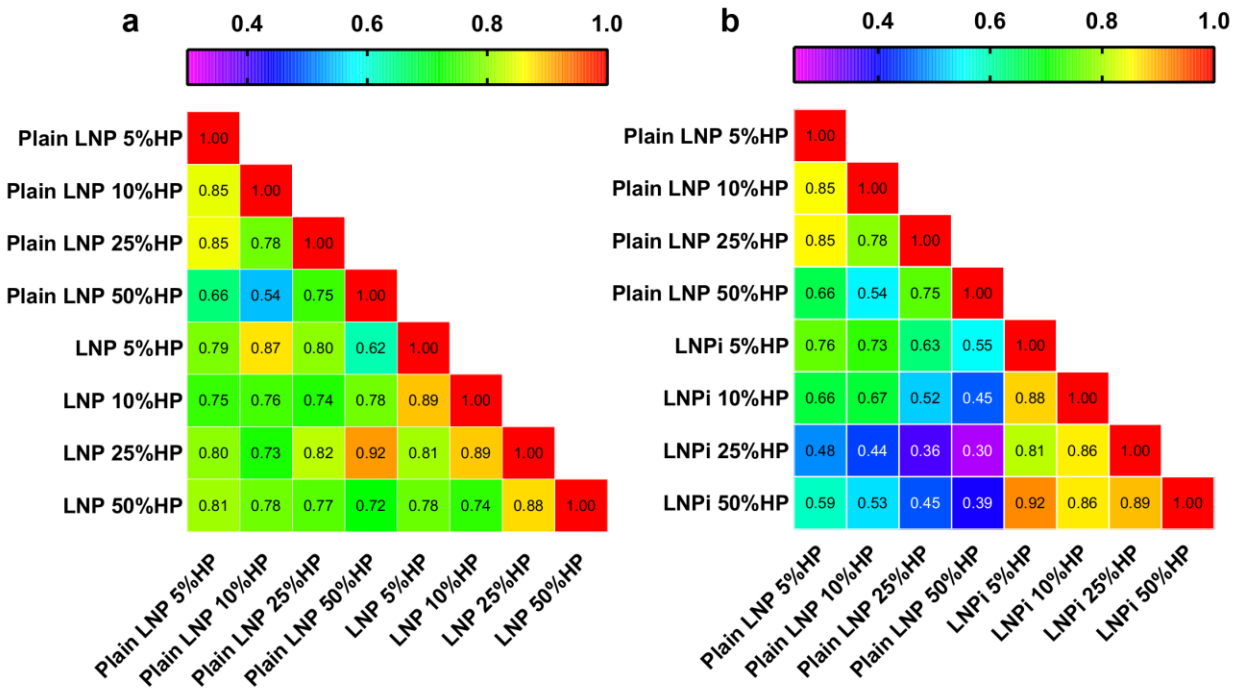

Supplementary Figure 8. (a) Heat map depicting the correlations among the 1D protein patterns surrounding plain LNP and LNP following a 1-hour incubation with escalating concentrations of human plasma (HP) ranging from 5% to 50%. (b) Heat map illustrating the correlations among the 1D protein patterns surrounding plain LNP and LNPi after 1-hour exposure to increasing concentrations of HP from 5% to 50%. Source data are provided as a Source Data file.

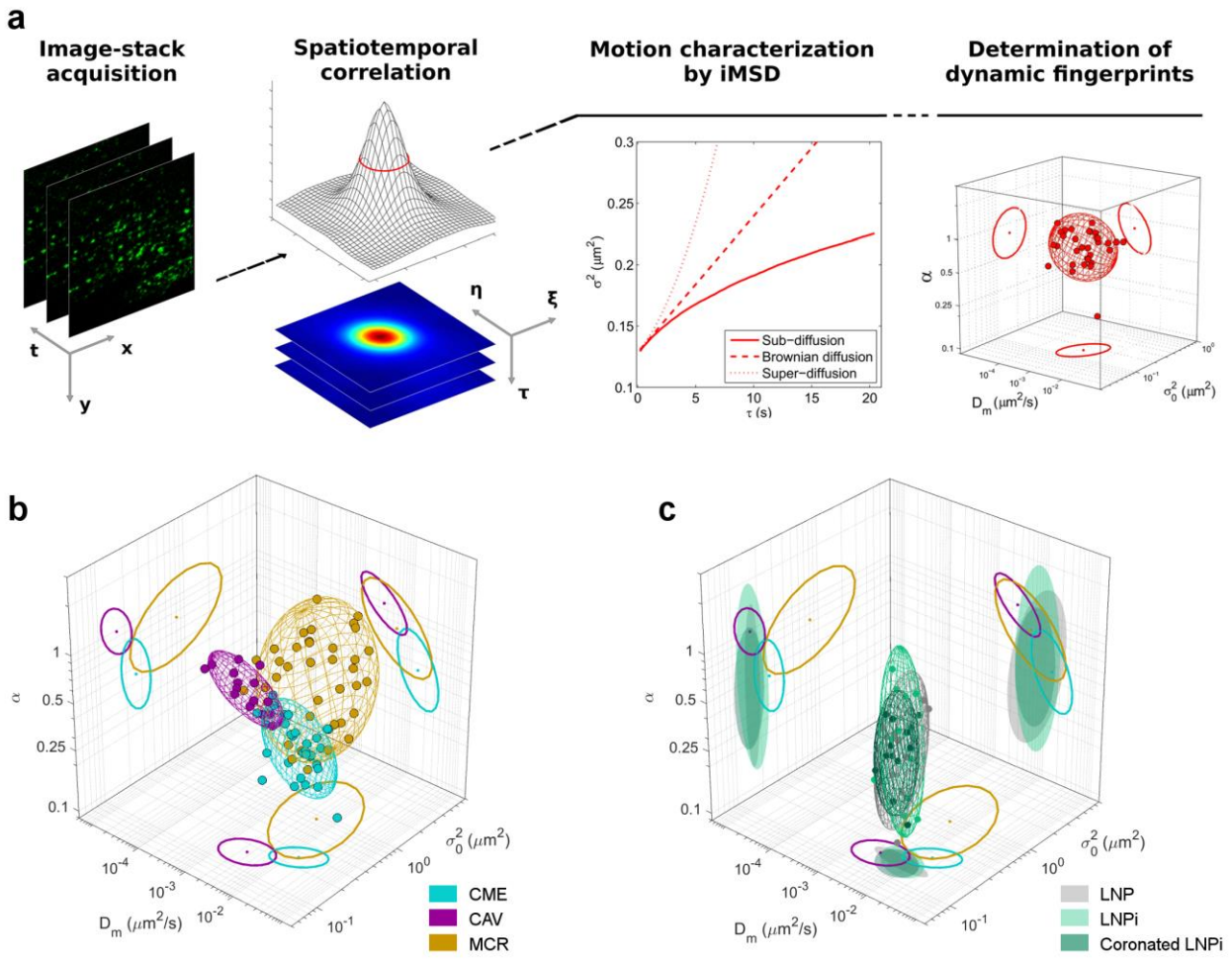

Supplementary Figure 9. (a) Schematic representation of the iMSD approach: acquisition of time-lapse confocal images, evaluation of the spatiotemporal correlation function followed by Gaussian fitting and iMSD curve computation. The fitting parameters are finally used as dynamic fingerprints of the investigated systems, graphically depicted in a 3D scatterplot. (b) 3D scatterplot of extracted parameters shows the differences in the dynamic properties of the endocytic vesicles, i.e. clathrin-coated vesicles (CME), caveolae (CAV), and macropinosomes (MCR). (c) 3D scatterplot of LNP, LNPi and coronated LNPi. Adapted with permission from Digiacomo et al. "Dynamic fingerprinting of sub-cellular nanostructures by image mean square displacement analysis". Scientific Reports, 2017. 7(1): p. 14836. Source data are provided as a Source Data file.

Protein Corona Stability in Excess Protein Conditions.

The stability of an artificial protein corona in a protein-rich environment (such as the bloodstream and the cytoplasm) is a key requirement for its effectiveness. This is because the corona stability influences its ability to maintain its composition and structure over time [1, 2]. In a protein-rich environment, various proteins are present that can potentially interact with the corona. If the corona is not stable, it may undergo structural changes or disintegrate, leading to alterations in its composition. This can have significant implications for the corona's functionality, including its ability to influence interactions between the NP and biological systems. As an example, Qin et al. [3] demonstrated that an intracellular protein corona (IPC) can form on nanoparticles once they are taken up by cells. This IPC has the potential to significantly impact the intracellular transport network of these NPs. A stable protein corona is therefore crucial for maintaining the specific interactions and properties that were designed or intended. It helps ensure that the corona continues to serve its intended purpose, whether it is to enhance biocompatibility, modulate cellular uptake by engaging specific receptors, or influence other aspects of nanoparticle behavior.

For this purpose, we prepared coronated LNP and LNPi at different plasma percentages. Each batch was aliquoted into two portions. The first represents the formulation as synthesized in the laboratory, constituting the system ready for in vivo applications. This batch was kept as is for 1 hour at 37 °C. Simultaneously, the second batch was exposed to 50% HP, i.e., the percentage of plasma commonly used in literature to mimic the injection of NPs into the circulatory system. Finally, we employed SDS-PAGE to compare the corona composition of coronated LNP and LNPi before and after plasma exposure (the electrophoretic gel is shown in **Supplementary Figure 6a**). First, we observe that the electrophoretic profiles of coronated LNP (light gray) change as a function of protein concentration. This first observation is in line with previous results obtained with lipid gene vectors[4], and other NP types[5]. After exposure to 50% high protein concentration (depicted in dark grey), LNP displayed very similar protein profiles. Comparatively, when comparing the protein profiles of coronated LNP created with 10% HP to those re-exposed to 50% HP, significant alterations were observed (see **Supplementary Figure 6b**).

Conversely, coronated LNPi (light green) showed minimal changes when subjected to increased protein concentration, and exposure to 50% high protein concentration (depicted in dark green) did not alter the protein profile. When comparing the protein profile of coronated LNPi created with 10% HP to that obtained upon exposure to 50% HP, no significant changes were observed (see **Supplementary Figure 6c**).

Collectively, these findings unequivocally illustrate that the artificial corona adsorbed onto LNPs can exhibit either stability or instability after exposure to excessive protein. Specifically, coronas formed up to a high protein concentration of 25% are unstable, whereas they remain stable when generated upon incubation in HP exceeding 25%. On the other hand, coronas of LNPi prepared at each concentration remain stable in an environment enriched with an excess of proteins.

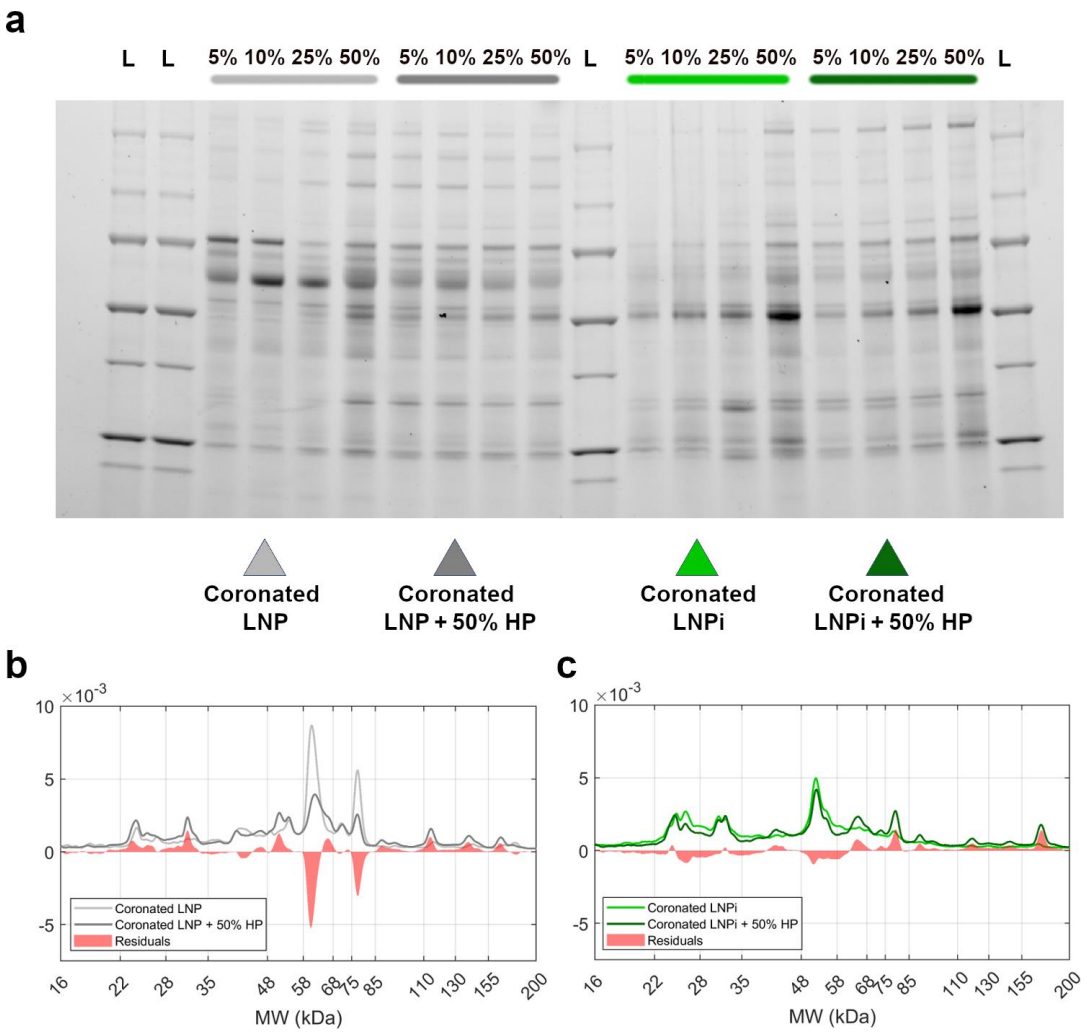

Supplementary Figure 10. (a) SDS-PAGE and profiles of LNP and LNPi exposed to different HP percentages (i.e., 5%, 10%, 25%, and 50%) indicated by light grey and light green respectively, and profiles of LNP and LNPi at different concentrations of HP then re-exposed to an excess of proteins (i.e., 50% HP) indicated with dark grey and green lines respectively. (b) protein profile of coronated LNP (made through 10% HP incubation) and coronated LNP after double exposure to 10% HP followed by 50% HP (dark gray line). (c) profiles of the coronated LNPi (light green) and of coronated LNPi re-exposed to 50% HP (dark green). Red lines represent the residual values of the two protein profiles. Source data are provided as a Source Data file.

Supplementary Table 3. A list of proteins composing the corona of LNP, LNPi and coronated LNPi incubated with 50% of human plasma (HP). Relative protein abundance (RPA) was calculated as reported in[5] and is reported as the mean of three independent replicates. Only proteins with an RPA > 0.1% on at least one corona have been included in the list.

Protein name	MW	pI	id	LNP RPA (%)	LNPi RPA (%)	LNPi HP RPA (%)
Serum albumin	69.4	5.97	ALB	45.35	35.66	36.83
Apolipoprotein A-I	30.8	5.52	APOA1	5.99	5.81	6.34
Haptoglobin	45.2	6.25	HP	4.03	4.14	4.02
Ig kappa chain C region	11.8	5.60	IGKC	3.74	7.07	5.47
Ig gamma-1 chain C region	36.1	8.05	IGHG1	3.61	3.28	3.87
Immunoglobulin lambda constant 3	11.3	6.90	IGLC3	3.5	5.42	6.47
Serotransferrin	77.1	6.80	TF	3.31	4.06	3.98
Ig gamma-3 chain C region	41.3	7.71	IGHG3	3.26	4.06	2.84
Alpha-1-antitrypsin	46.7	5.33	SERPINA1	2.24	2.3	2.16
Fibrinogen alpha chain	95.0	5.73	FGA	1.64	0.87	1.25
Ig alpha-1 chain C region	37.7	6.17	IGHA1	1.57	1.57	1.83
Fibrinogen gamma chain	51.5	5.32	FGG	1.52	1.85	1.77
Apolipoprotein A-II	11.2	6.44	APOA2	1.48	1.99	4.15
Apolipoprotein C-III	10.9	5.12	APOC3	1.44	1.09	0.68
Fibrinogen beta chain	55.9	8.11	FGB	1.08	1.51	1.19
Ig gamma-2 chain C region	35.9	7.38	IGHG2	1.03	1.69	1.36
Alpha-1-acid glycoprotein 1	23.5	4.80	ORM1	1.00	1.47	0.94
Ig gamma-4 chain C region	35.9	7.10	IGHG4	0.93	0.21	0.33
Complement C3	187.2	6.10	C3	0.81	1.10	1.11
Hemopexin	51.7	6.67	HPX	0.79	1.18	1.14
Apolipoprotein D	21.3	4.93	APOD	0.74	0.26	0.35
Ig mu chain C region	49.4	6.44	IGHM	0.70	1.07	0.82
Alpha-2-macroglobulin	163.3	6.15	A2M	0.58	0.69	0.68
Apolipoprotein C-I	9.3	8.76	APOC1	0.53	0.52	0.69
Vitamin D-binding protein	52.9	5.30	GC	0.40	0.30	0.37
Ig heavy chain V-III region JON	12.9	9.47		0.40	0.44	0.5
Apolipoprotein E	36.2	5.54	APOE	0.34	0.48	0.32
Apolipoprotein A-IV	45.4	5.18	APOA4	0.33	0.61	0.4
Vitronectin	54.3	5.52	VTN	0.31	0.16	0.11
Alpha-2-HS-glycoprotein	39.3	5.44	AHSG	0.28	0.34	0.3
Beta-2-glycoprotein 1	38.3	7.78	APOH	0.27	0.26	0.27
Apolipoprotein C-II	11.3	4.50	APOC2	0.27	0.30	0.41
Ig kappa chain V-III region VG	12.6	5.04	IGKV3D-11	0.25	0.21	0.09
Immunoglobulin heavy variable 3-15	13.1	8.59	IGHV3-15	0.24	0.19	0.12
Ig heavy chain V-III region KOL	13.1	8.02	IGHV3-66	0.24	0.18	0.22

Ig kappa chain V-III region B6	12.6	9.37		0.22	0.26	0.18
Hemoglobin subunit beta	16.0	6.96	HBB	0.22	0.25	0.14
Platelet factor 4	10.8	8.53	PF4	0.22	0.06	0.07
Antithrombin-III	52.6	6.40	SERPINC1	0.20	0.28	0.28
Alpha-1-acid glycoprotein 2	23.6	4.91	ORM2	0.20	0.54	0.22
Complement C4-B	192.8	6.95	C4B	0.19	0.20	0.25
Transthyretin	15.9	5.50	TTR	0.19	0.13	0.13
Alpha-1-antichymotrypsin	47.7	5.26	SERPINA3	0.19	0.31	0.39
Ig kappa chain V-III region POM	12.5	5.65	IGKV3D-7	0.19	0.46	0.21
C4b-binding protein alpha chain	67.0	7.01	C4BPA	0.18	0.18	0.15
Complement factor H	139.1	6.27	CFH	0.17	0.17	0.16
Alpha-1B-glycoprotein	54.3	5.60	A1BG	0.16	0.29	0.20
Plasminogen	90.6	6.94	PLG	0.16	0.15	0.18
Kininogen-1	72.0	6.48	KNG1	0.15	0.16	0.13
Ig kappa chain V-IV region	13.4	4.95	IGKV4-1	0.15	0.05	0.07
Immunoglobulin kappa variable 2-29	13.1	5.82	IGKV A18	0.13	0.00	0.03
Hemoglobin subunit alpha	15.3	8.86	HBA1	0.13	0.13	0.23
C-reactive protein	25.0	5.39	CRP	0.12	0.02	0.01
Prothrombin	70.0	5.62	F2	0.12	0.18	0.15
Apolipoprotein B-100	515.6	6.73	APOB	0.11	0.12	0.07
Inter-alpha-trypsin inhibitor heavy chain H2	106.5	6.54	ITIH2	0.10	0.12	0.11
Complement factor B	85.5	6.73	CFB	0.10	0.12	0.13
Complement C1q subcomponent subunit B	26.7	8.61	C1QB	0.08	0.24	0.17
Ceruloplasmin	122.2	5.44	CP	0.08	0.15	0.16

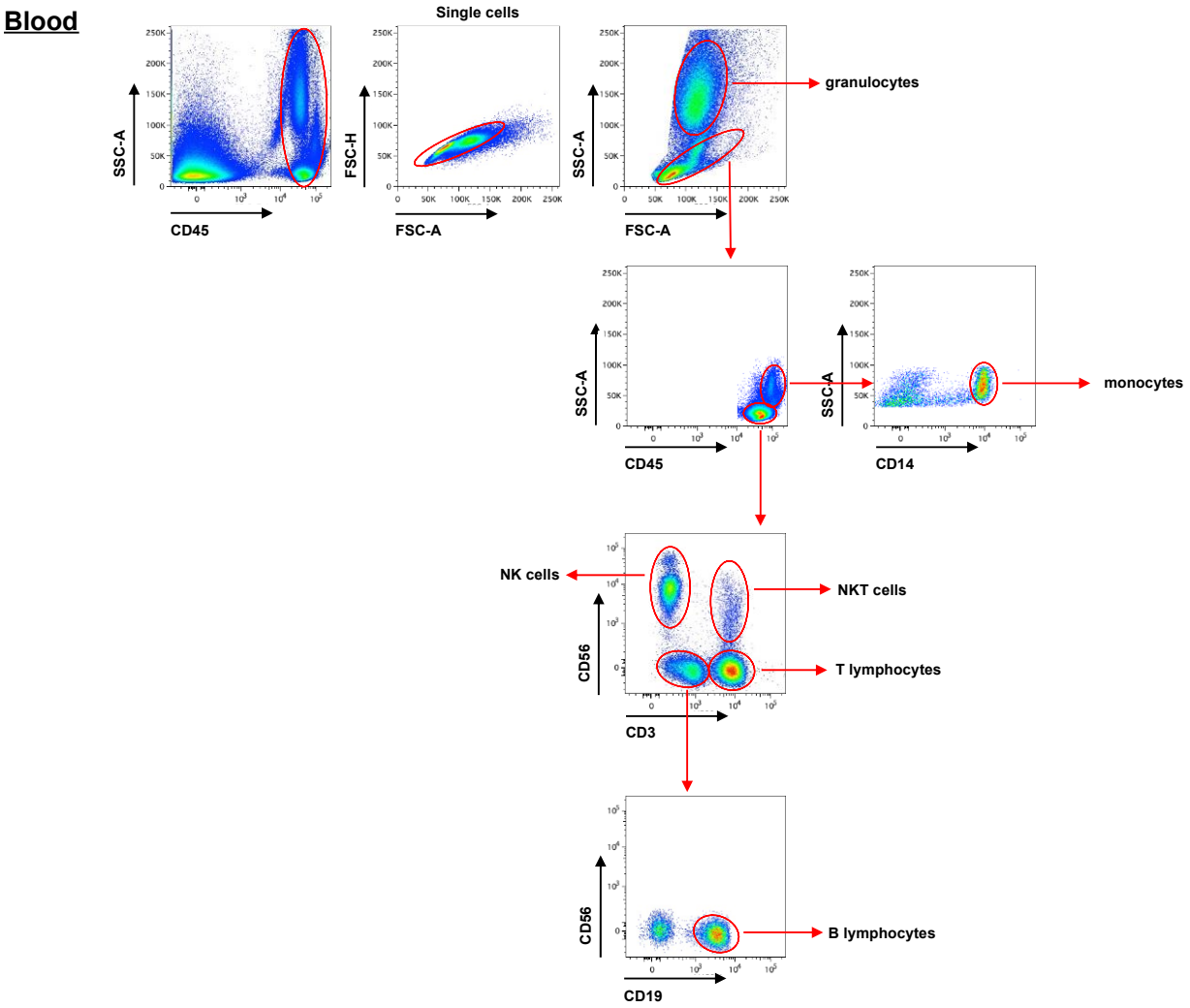

Supplementary Figure 11. Representative dot plots of human leucocyte populations in the blood dissected by gating on CD45^{+} single cells as indicated. (a) Exclusion of residual red blood cells by gating on CD45+ population (αCD45PECy7); (b) exclusion of doublets by gating on FSC-A vs FSC-H; (c) elimination of debris by gating on FSC-A vs SSC-A. Granulocytes identified by gating on SSC-Ahigh. Other leukocyte populations identified by gating on: (d) CD45+CD14+ (monocytes; αCD45PECy7/ αCD14APC); (e) CD45+CD3-CD56+ (NK cells; αCD45PECy7+/ αCD3BV410/ αCD56PE); CD45+CD3+CD56- (T lymphocytes; αCD45PECy7/ αCD3BV410/ αCD56-PE): CD45+CD3+CD56+ (NKT cells; αCD45PECy7/ αCD3BV410/ αCD56PE); (f) CD45+CD3-CD56-CD19+ (B lymphocytes; αCD45PECy7/ αCD3BV410/ αCD56PE/ αCD19/BV450).

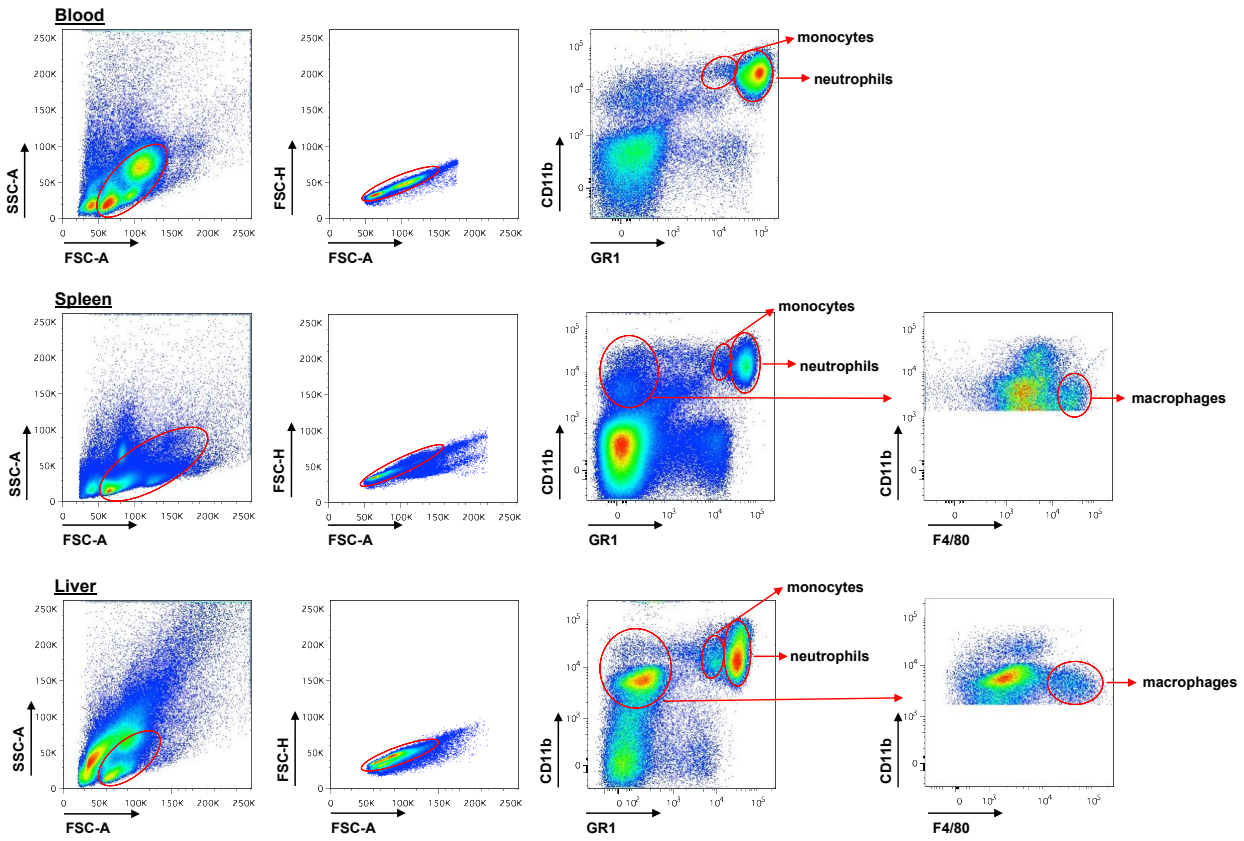

Supplementary Figure 12. Representative dot plots of phagocyte populations in the blood, spleen, and liver dissected by gating on CD11b+GR1low (monocytes), CD11b GR1high (neutrophils) and CD11b+GR1-F4/80+ (macrophages). The gating on FSC-A vs SSC-A to eliminate debris followed by gating on FSC-A vs FSC-H to exclude doublets is shown.

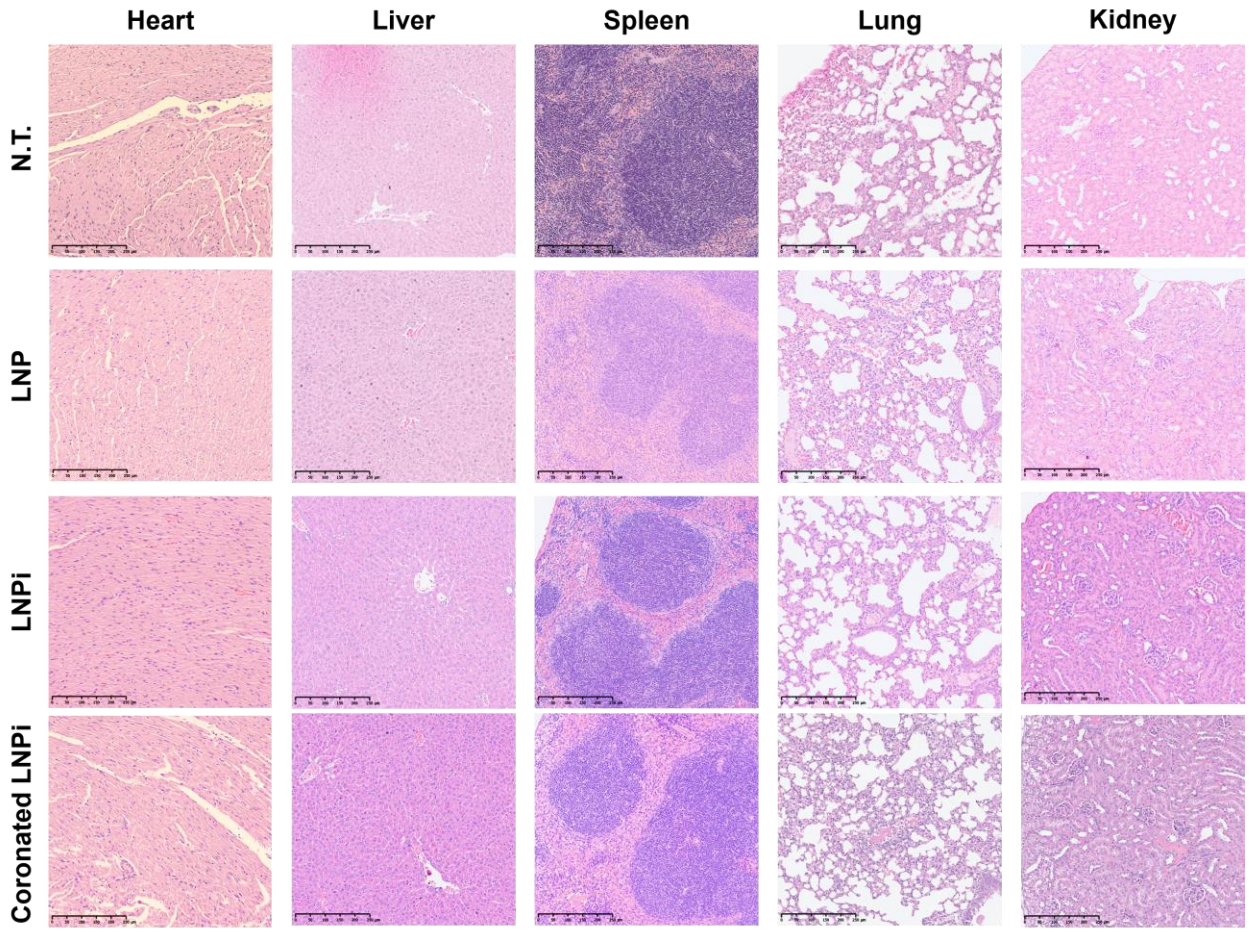

Supplementary Figure 13. Histopathological analysis of heart, kidney, liver, spleen, lung, and kidney tissues after systemic injection of LNP, LNPi and coronated LNPi in 8-10 weeks-old C57BL/6 female mice (n=4/group). Representative images of organ sections stained with hematoxylin and eosin 24 h post-injection are shown. N.T. not-treated mice. Original magnification 10X. Scale bar 250 µM.

Supplementary Table 4. Material characterization Question	**Yes**	**No**
1.1 Are "**best reporting practices**" **available** for the nanomaterial used?	Not applicable	
1.2 If they are available, **are they used**? If not available, ignore this question and proceed to the next one.		
1.3 Are extensive and clear instructions reported detailing all steps of **synthesis** and the resulting **composition** of the nanomaterial?	√	
1.4 Is the **size** (or **dimensions**, if non-spherical) and **shape of** the nanomaterial reported?	√	
1.5 Is the **size dispersity** or **aggregation** of the nanomaterial reported?	√	
1.6 Is the **zeta potential** of the nanomaterial reported?	√	
1.7 Is the **concentration (mass/volume)** of the nanomaterial reported?	√	
1.8 Is the amount of any **drug loaded** reported? 'Drug' here broadly refers to functional cargos (*e.g.*, proteins, small molecules, nucleic acids).	√	
1.9 Is the **targeting performance** of the nanomaterial reported, including **amount** of ligand bound to the nanomaterial if the material has been functionalised through addition of targeting ligands?	Not applicable	
1.10 Is the **label signal** per nanomaterial/particle reported? For example, fluorescence signal per particle for fluorescently labeled nanomaterials.	√	
1.11 If a material property not listed here is varied, has it been **quantified**?	Not applicable	
1.12 Were characterizations performed in a **fluid mimicking biological conditions**?	√	
1.13 Are details of how these parameters were **measured/estimated** provided?	√	

Supplementary Table 5. Biological characterization Question	**Yes**	**No**
2.1 Are **cell seeding details**, including **number of cells plated, confluency at start of experiment,** and **time between seeding and experiment** reported?	√	
2.2 If a standardised cell line is used, are the **designation and source** provided?	√	
2.3 Is the **passage number** (total number of times a cell culture has been subcultured) known and reported?	Not applicable	
2.4 Is the last instance of **verification of cell line** reported? If no verification has been performed, is the time passed and passage number since acquisition from trusted source (*e.g.*, ATCC or ECACC) reported? For information, see *Science* **347** (2015) 938; http://doi.org/10.1126/science.347.6225.938	No	
2.5 Are the results from **mycoplasma testing** of cell cultures reported?	No	
2.6 Is the **background signal of cells/tissue** reported? (*E.g.*, the fluorescence signal of cells without particles in the case of a flow cytometry experiment.)	√	
2.7 Are **toxicity studies** provided to demonstrate that the material has the expected toxicity, and that the experimental protocol followed does not?	Not applicable	
2.8 Are details of media preparation (**type of media, serum,** any **added antibiotics**) provided?	√	
2.9 Is a **justification of the biological model** used provided? For examples for cancer models, see *Cancer Res.* **75** (2015) 4016; http://doi.org/10.1158/0008-5472.CAN-15-1558, and *Mol. Ther.* **20** (2012) 882; http://doi.org/10.1038/mt.2012.73, and *ACS Nano*	√	

11 (2017) 9594; http://doi.org/10.1021/acsnano.7b04855	
2.10 Is characterization of the **biological fluid** (*ex vivo*/*in vitro*) reported? For example, when investigating protein adsorption onto nanoparticles dispersed in blood serum, pertinent aspects of the blood serum should be characterised (*e.g.*, protein concentrations and differences between donors used in study).	√
2.11 For **animal experiments**, are the ARRIVE guidelines followed? For details, see *PLOS Biol.* **8** (2010) e1000412; http://doi.org/10.1371/journal.pbio.1000412	√

Supplementary Table 6. Experimental details Question	**Yes**	**No**
3.1 For cell culture experiments: are **cell culture dimensions** including **type of well**, **volume of added media**, reported? Are cell types (*i.e.*; adherent *versus* suspension) and **orientation** (if non-standard) reported?	√	
3.2 Is the **dose of material administered** reported? This is typically provided in nanomaterial mass, volume, number, or surface area added. Is sufficient information reported so that regardless of which one is provided, the other dosage metrics can be calculated (*i.e.* using the dimensions and density of the nanomaterial)?	√	
3.3 For each type of imaging performed, are details of how **imaging** was performed provided, including details of **shielding, non-uniform image processing**, and any **contrast agents** added?	√	
3.4 Are details of how the dose was administered provided, including **method of administration, injection location, rate of administration,** and details of **multiple injections**?	√	
3.5 Is the methodology used to **equalise dosage** provided?	√	

3.6 Is the **delivered dose** to tissues and/or organs (*in vivo*) reported, as % injected dose per gram of tissue (%ID g_{-1})?	√
3.7 Is **mass of each organ/tissue measured** and **mass of material** reported?	Not applicable
3.8 Are the **signals of cells/tissues with nanomaterials** reported? For instance, for fluorescently labeled nanoparticles, the total number of particles per cell or the fluorescence intensity of particles + cells, at each assessed timepoint.	Not applicable
3.9 Are **data analysis details**, including **code used** for analysis provided?	√
3.10 Is the **raw data** or **distribution of values** underlying the reported results provided? For examples, see *R. Soc. Open Sci.* **3** (2016) 150547; http://doi.org/10.1098/rsos.150547, https://opennessinitiative.org/making-your-data-public/, http://journals.plos.org/plosone/s/data-availability, and https://www.nature.com/sdata/policies/repositories	√

Supplementary Table 7. SAS data collection table.

SAS data collection parameters
Source, instrument Austrian SAXS beamline @ ELETTRA-Sicnrotrone Trieste
Wavelength (Å) 1.54
Beam geometry: size<. 0.3 x 2 mm sample-to-detector distance: 1532.5 mm
q-measurement range (nm^{-1}): 0.08 – 4.65
Basis for normalization to constant counts: Photodiode in beamstop
Method for monitoring radiation damage: Multiple frames check of pattern stability
Exposure time, number of exposures: 20 s x 10
Sample configuration including path length and flow rate where relevant: 1.5 mm Quarzglass capillaries
Sample temperature (ºC) R.T.
Software employed for SAS data reduction, analysis and interpretation
SAS data reduction to sample–solvent scattering, and extrapolation, merging, desmearing *etc*. as relevant

References

1. Tenzer, S. et al. Rapid formation of plasma protein corona critically affects nanoparticle pathophysiology. *Nat Nanotechnol* **8**, 772-781 (2013).
2. Barrán-Berdón, A.L. et al. Time evolution of nanoparticle–protein corona in human plasma: relevance for targeted drug delivery. *Langmuir* **29**, 6485-6494 (2013).
3. Qin, M. et al. Proteomic analysis of intracellular protein corona of nanoparticles elucidates nano-trafficking network and nano-bio interactions. *Theranostics* **10**, 1213 (2020).
4. Caracciolo, G. et al. Evolution of the protein corona of lipid gene vectors as a function of plasma concentration. *Langmuir* **27**, 15048-15053 (2011).
5. Monopoli, M.P. et al. Physical− chemical aspects of protein corona: relevance to in vitro and in vivo biological impacts of nanoparticles. *Journal of the American Chemical Society* **133**, 2525-2534 (2011).